2026 IEEE International Conference on Robotics and Automation (ICRA 2026)
June 1-5, 2026. Vienna, Austria

Autonomous Robot-Assisted Ureteroscopy (ARA-URS) for the Treatment of Kidney Stones

Sarvesh Saini*[1], Julio Ojalvo[1], Jonathan E. Katz[2], and Ubbo Visser[1]

Abstract— **We present a supervised autonomous robot-assisted ureteroscopy (ARA-URS) system for the treatment of kidney stones, integrated with a digital-twin (DT). A three degrees of freedom (3-DOF) robotic system was developed to actuate a Wolf disposable ureteroscope, enabling the ARA-URS to autonomously position the ureteroscope for laser lithotripsy procedures. The DT of the robotic system was developed to enable the generation of diverse synthetic intraoperative scenarios, which are used to train vision and control models for improved precision in ARA-URS. By mapping joint motion to virtual counterparts via precise physics simulation, the system ensures realistic representation and reliable validation. This framework's performance was assessed with particular focus on endoscopic tip positioning. Initial in-air simulation experiments demonstrated root mean square error (RMSE) values of (1.871, 1.725, 1.194) mm in the x-, y-, and z-directions, respectively, computed as the deviation between the desired laser target position and the achieved ureteroscope tip position. Corresponding real-world experiments yielded RMSE values of (5.029, 3.919, 6.681) mm. The comparison between simulated and physical experiments indicates that the DT is able to reproduce the motion behavior of the physical system with good agreement. Further benchtop and simulation experiments demonstrated the system's capacity for stone targeting (quantified by the percentage of the image occluded by stone). In digital simulation, the ureteroscope achieved 88.77% average stone area coverage, while in the benchtop model, coverage averaged 59.04%. Together, this proof of concept highlights the potential of DT technology in robotic-assisted URS, offering a scalable and interactive platform for refining surgical techniques.**

Index Terms— **Robot-assisted ureteroscopy, digital twin, medical robotics, surgical automation, sensor-based navigation.**

I. Introduction

Ureteroscopy with laser lithotripsy (URS) remains the most commonly performed procedure for renal calculi, commonly known as kidney stones, measuring $\leq$ 20 mm [1]. However, the surgery is complex to master with an estimated learning curve of 60 surgeries [2]. Furthermore, even in expert hands, patient outcomes remain suboptimal. Despite several advances, post-operative stone-free rates in randomized controlled trials remain only approximately 50% [3]–[5]. For those with residual stone, approximately 20%-30% will suffer another kidney stone-related episode over the ensuing 12-18 months [6], [7]. Additionally, complication rates remain around 10%- 20% and range in severity from pain and blood in the urine to sepsis and need for urgent re-intervention [5], [8].

*Corresponding author: sarveshs@cs.miami.edu. [1]Dept. of Computer Science, Univ. of Miami, FL, USA. [2]Desai Sethi Urology Institute, Univ. of Miami, FL, USA.

Furthermore, the ergonomics and radiation exposure from manual URS are both taxing and a dangerous work exposure for surgeons. Approximately 64% of endourologists report orthopedic problems, and the percentage correlates with surgical volume [9]. Additionally, during manual URS, the surgeon is positioned in close proximity to the fluoroscopic arm and radiation source, leading to increased risk of cataracts and stochastic malignancy. Thermoluminescent dosimeters revealed that the surgeon's lower leg (unprotected by a lead apron) receives approximately 12 μGy, while the eyes receive approximately 2 μGy per procedure [10].

To improve upon human limitations in precision and control and to optimize surgeon ergonomics while minimizing radiation exposure, robotic-assisted ureteroscopy systems have been developed [11], [12]. The Roboflex™Avicenna was developed in the 2010s, with promising early human subject outcomes [11]; however adoption has been limited due to questions regarding the increased cost and complexity of the surgical setup, considering only minimal improvements in clinical outcomes [13]. More recently, the easyUretero™system was developed with added features, including respiratory syncing to further increase stone ablation efficiency and stone fragment size alerts to minimize the risk of ureteral or renal trauma associated with attempting to remove too large a stone fragment from the kidney [14]. However, this robotic system is not yet FDA cleared and may face similar challenges to widespread adoption as the Roboflex™.

In contrast, a robotic surgical assistant may be more widely adopted, as it can potentially optimize surgical performance while also automating the tedious aspects of the procedure. Furthermore, autonomous robotic actions offer the potential to offload repetitive sub-tasks, thereby reducing cognitive burden and maintaining consistency, while allowing surgeons to focus on higher-level decision-making [15]. black Recent developments in robotic and biologic physics-based simulation engines, such as Gazebo [16], MuJoCo [17] or NVIDIA's Isaac Sim™ [18], have provided novel opportunities for surgical training for both surgical trainees and autonomous robots. In orthopedic surgery, optimization of knee arthroscopy has been attempted first in simulation and then via extended reality in humans [19]. Similarly, a simulation suturing environment has been developed to facilitate robotic suturing both for surgical trainees and for algorithms to enable autonomous action [20].

black We propose a novel ARA-URS system with a DT (in Fig. 1) to generate diverse surgical scenarios that sup-

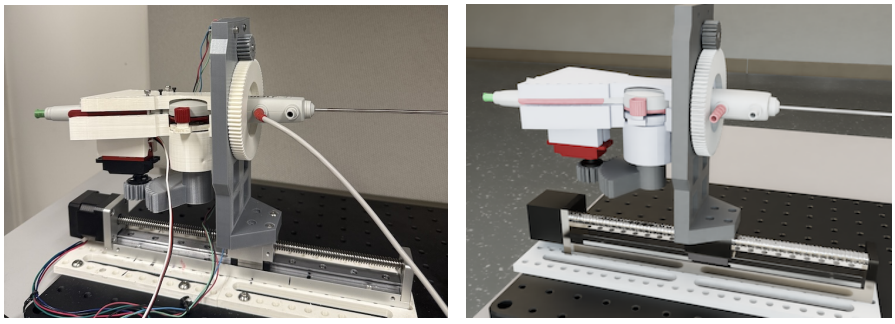

(a) ARA-URS Robot (b) DT in NVIDIA Isaac Sim

Fig. 1: ARA-URS alongside its DT developed in NVIDIA Isaac Sim.

port the development of computer vision and motor control algorithms for autonomous task completion. Unlike prior RA-URS systems built around fully flexible ureteroscopes, we selected the recently developed Wolf RIWO Digital Ureteroscope [21], which features a semi-rigid shaft with a fully flexible tip. This design streamlines the RA-URS system by eliminating the need to stabilize and track the floppy, flexible shaft. Importantly, it also obviates the need for a ureteral access sheath, which is only feasible in about 90% of patients [22] and associated with trauma in nearly 50% [23]. In addition, this scope offers a dedicated outflow channel that allows increased irrigation inflow and improved visualization while maintaining safe intra-renal pressures, along with direct in-scope suction for efficient dust removal. Taken together, an ARA-URS system built around this scope maximizes the potential to safely render the patient stone-free.

We conduct two complementary sets of experiments to evaluate and validate the ARA-URS system. First, in-air simulation studies were performed to assess ureteroscopic tip control, confirming the integrity of both the DT and the benchtop ARA-URS platform. Second, an initial autonomous task – navigating the ureteroscope tip through the renal collecting system toward a target kidney stone – was implemented using a novel computer vision pipeline and validated in both the real-world prototype and its DT.
The major contributions of this work are as follows:

1) Design and development of a novel ARA-URS system for the treatment of renal stones.
2) Creation of a high-fidelity DT using NVIDIA Isaac Sim and its validation in benchtop experiments.
3) Synchronization testing of an initial autonomous task using a novel computer vision pipeline, validated in both simulated and real environments.

The article is organized as follows: Section I introduces the study and reviews the literature on robotics in ureteroscopy, with particular emphasis on simulation-based approaches for computer vision and motor control. Section II (Methods and Materials) provides a system overview, including the development of the ARA-URS and its DT, covering both simulation and physical implementation. Section III presents the kinematics of the 3-DOF ARA-URS, along with validation experiments comprising in-air kinematic kinematic accuracy assessment and in-vitro stone targeting in a fabricated kidney model with calcium oxalate stones. Section IV discusses the experimental results and their implications in detail. Finally, Section V concludes the work and outlines directions for future research.

II. Methods and Materials

The development of the ARA-URS with its DT began with the design of individual components and their assembly in SolidWorks. The URDF model of the RA-URS was exported to Isaac Sim in parallel with the real-world development, which involved integrating the ureteroscope, actuators, and 3D-printed components.

A. Design of ARA-URS

The components requiring special attention during the design process included the ureteroscope, motors, twisted clamps, and holders for mounting the motors onto the ureteroscope. These components were designed using Rhino software, leveraging its rendering capabilities. The models created in Rhino were imported into SolidWorks as `.3dm` files for assembly and into Isaac Sim as `.usd` files, where physics, and colliders were defined. Visual appearance and textures were further refined in USD Composer.

As shown in Fig. 2, the development phases of the ureteroscope follow a structured workflow encompassing geometric modeling, cross-platform integration, and physics-based simulation. Using physical measurements, photographs, and supplier-provided documentation (Fig. 2(a)), a detailed model is constructed in Rhino with SubD surfaces as shown in Fig. 2(b) and (c), iteratively refined through shading checks, Boolean operations, and filleted connections before being exported to SolidWorks. The geometries are subsequently imported into NVIDIA Isaac Sim through the Universal Scene Description (USD) framework, enabling modular assembly via Payloads and visual refinement in NVIDIA USD Composer. Tip deflection is modeled as a seven-segment articulated chain with revolute joints (Fig. 2(d)), where the total deflection angle is distributed across all joints to capture realistic bending behavior. A virtual camera is attached to ensure accurate viewpoint matching, while hierarchical structuring at the assembly level allows parent–child

relationships to govern translation, shaft rotation, and tip deflection, all controlled through the Action Graph with an integrated reset function. In an experiment scenario, an alternative approach is to regulate the distributed joint angles using stiffness and damping, thereby achieving smooth and controlled tip motion. Simulation stability is further enhanced by increasing the physics parameters, minimum simulation frame rate, and time steps per second from 30 to 5,000, yielding a robust and realistic DT.

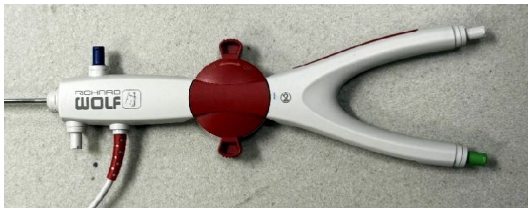

(a) Wolf RIWO Digital Ureteroscope

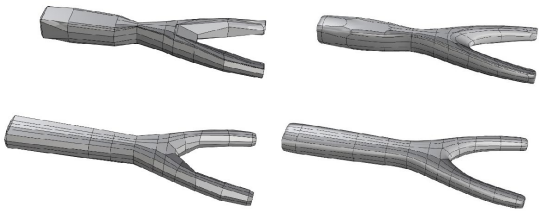

(b) SubD modelling of the Ureteroscope

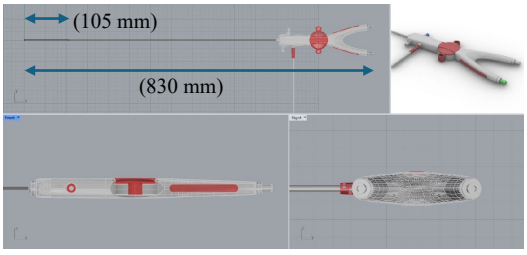

(c) 3D model of Ureteroscope in Rhino

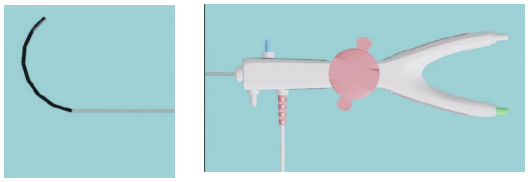

(d) Ureteroscope tip action with 7-segments

Fig. 2: Development of ureteroscope digital model.

The motors used in the system were also modeled in Rhino, referencing photographs and manufacturer specifications to ensure accurate dimensions. A rendered model of a motor is shown in Fig. 3(a), where the Fillet Edge feature was applied to create realistic corners and gaps, ensuring consistency between the physical design and the DT. Considering the uneven surface of the ureteroscope, which is traditionally actuated by the surgeon, direct actuation in an automated task is challenging. To address this, a twisted clamp (Fig. 3(b)) and custom holders (Fig. 3(c)) were designed to securely mount the ureteroscope, enabling precise actuation of its tip using the motor. All the rendered and modeled components – including the ureteroscope, actuators, benchtop, connecting plate, stand, clamps, holders, and gears – are assembled in SolidWorks.

From this assembly, a URDF model is generated, as depicted in Fig. 4. Instead of manually assembling geometries, defining joints, and configuring physics parameters within Isaac Sim, the URDF provides a standardized description of the robot's structure that can be directly imported into the simulator. This approach accelerates the setup process and minimizes human error when specifying complex kinematic chains, joint limits, inertial properties, and collision geometries. By serving as a single source of truth for both structural and dynamic properties, the URDF streamlines the pipeline from design to simulation and enables reproducible, high-fidelity DTs within Isaac Sim.

(a) Rendered Motor

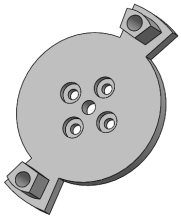

(b) Twister clamp

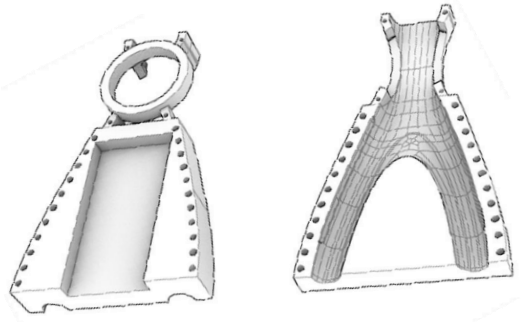

(c) Upper and lower holder for ureteroscope

Fig. 3: Motor, clamp and holder design for ARA-URS.

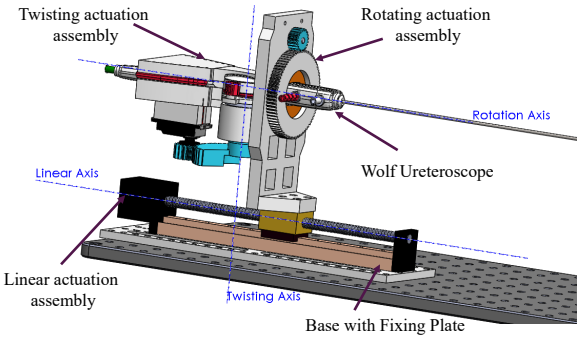

Fig. 4: Design with unified robot description format (URDF) with axes of 3-DOF for ARA-URS.

B. Development of Real-World RA-URS

The ARA-URS experimental setup includes a Wolf RIWO Digital Ureteroscope with a semi-rigid shaft and fully flexible tip, actuated by a NEMA 14 stepper motor providing a 200 mm stroke for linear insertion and retraction. Full ureteroscope insertion (∼250–300 mm) is performed manually by the surgeon, while the robot provides fine positioning once the scope is near the stone. Since the working distance during ureteroscopy is typically 20–50 mm, the 200 mm translational range is sufficient for autonomous targeting and adjustment. A 0.9° stepper motor for rotation, and an ANNIMOS 25 kg digital servo motor to control twisting degrees of freedom, thereby enabling precise and complex maneuvering within the urinary tract. Vision-based tip tracking, using a high-resolution endoscopic camera and image-processing algorithms, provides continuous feedback for accurate control. Two perpendicular cameras were employed to obtain the world position for in-air tracking. The actuation system is coordinated by a microcontroller, which synchronizes all actuators and leverages kinematic modeling to translate desired tip positions into precise motor commands. As shown in Fig. 5(a), the developed setup integrates

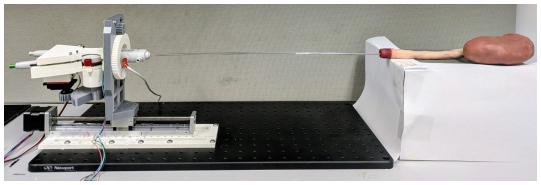

(a) Real ARA-URS experimental setup with kidney model and stone

(b) Synthetic kidney model

(c) Kidney stone

Fig. 5: ARA-URS experimental setup with kidney (ren) and kidney stone (renal calculi).

the ureteroscope assembly with a synthetic kidney (Fig. 5(b)) and kidney stone (Fig. 5(c)). The kidney model was placed on a stable platform, and the kidney stone was positioned in different poles of the kidney using a retrieval basket without any adhesive fixation. In the validation experiments, in-air kinematic calibration was performed for both the real-world and DT ARA-URS. The tip position was tracked using two cameras placed along perpendicular axes to determine its true world coordinates. In the subsequent in-vitro stone targeting experiments, the ureteroscope's endoscopic camera was used to identify the stone's position, and inverse kinematics was applied to compute the joint angles for the three actuators. These joint angles were then used to actuate the system, guiding the ureteroscope tip through the renal collecting system toward the target stone.

C. Development of DT of RA-URS

A DT of the RA-URS (Fig. 6(a)) is created in NVIDIA Isaac Sim using the `.stl` files of CAD models exported from SolidWorks through the URDF framework. Since the URDF export provides geometry in `.stl` format with only basic texture information, the ureteroscope developed natively in Isaac Sim (as described in the previous subsection) is substituted into the imported model. All components are then enhanced with appropriate color and texture attributes to replicate the physical system, yielding a high-fidelity DT. Real-time synchronization between the physical and virtual systems is achieved through joint mapping and motion tracking. The Kinematic Accuracy Assessment of the URS Robot and task-navigation experiments, presented in the next section, are conducted to assess the correspondence between the real prototype and its DT, thereby examining the fidelity of the simulated environment.

The kidney model [24], [25] is developed from patient CT scans [26], which are first converted into `.obj` files and imported into Blender for refinement. Distortions caused by patient motion during scanning are corrected through extensive editing of vertices, edges, and surfaces, with the Laplacian Smooth Modifier in Blender applied to further enhance surface continuity, thereby reconstructing an anatomically accurate renal pelvis and ureter—regions critical for simulating stone removal. We created custom textures from surgical images and applied them in Blender using UV mapping and shader nodes, reproducing the mucosal appearance of the ureter, renal pelvis, and calyces. This process produced a visually and anatomically realistic kidney model that serves as the surgical environment for robotic simulation. Different internal and external views of the rendered kidney are depicted in Fig. 6(b).

Kidney stone models are developed to capture clinically relevant variations in shape, size, and surface morphology, enabling anatomically realistic DTs for surgical simulation. Real patient samples and medical images serve as references for modeling the most common kidney stones: calcium oxalate, calcium phosphate, uric acid, and struvite. A custom light-box setup with two 4K UHD cameras (EMEET C950), a NEMA 14 stepper motor, and a 3D-printed holder enables controlled multi-angle acquisition. 40 images per stone (twenty from each camera) are captured at 18° increments and processed in Adobe's Substance 3D Sampler to generate 3D reconstructions. Rendered kidney stones of uric acid (UA), calcium oxalate monohydrate (COM), calcium hydrogen phosphate dihydrate (CHPD), and magnesium ammonium phosphate hexahydrate/carbonate apatite (MAPH/CA) types are shown in Fig. 6(b).

III. Experiments and Results

To evaluate the consistency between the real-world ARA-URS system and its digital twin (DT), two experiments were conducted: (a) *Kinematic accuracy assessment of the URS Robot*, and (b) *In-vitro stone targeting experiment*.

A. Kinematic Accuracy Assessment of the URS Robot

To validate calibration of both the real-world and DT models of the ARA-URS system, an in-air kinematic accuracy assessment experiment was performed. Thirty random points

(a) DT of ARA-URS

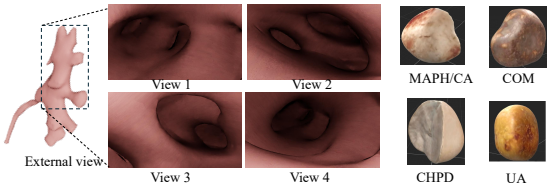

(b) Rendered kidney and kidney stones

Fig. 6: DT of ARA-URS developed for NVIDIA Isaac Sim.

were selected within the reachable workspace of the robotic system in both the real-world setup (Fig. 7(a)) and the DT simulation. For each point, the inverse kinematics model was used to compute the corresponding joint angles, which were then executed on both systems to directly compare the desired and actual tip positions.

The forward kinematics of the actuated joints and continuum section were used to compute the tip position $\boldsymbol{p}_t = (x_t, y_t, z_t)^T$:

$$x_t = \cos\theta_2 \, L_c \, \frac{1-\cos\theta_c}{\theta_c}, \tag{1}$$

$$y_t = \sin\theta_2 \, L_c \, \frac{1-\cos\theta_c}{\theta_c}, \tag{2}$$

$$z_t = L_1 + d_1 + L_c \, \frac{\sin\theta_c}{\theta_c}, \tag{3}$$

where $L_c = 105\,\text{mm}$ is the continuum segment length, $\theta_c \in \left[-\frac{5\pi}{3}, \frac{5\pi}{3}\right]$ is the bending angle, $\theta_2 \in [-\pi, \pi]$ is the rotation angle, $L_1 = 565\,\text{mm}$ is the fixed offset, and $d_1 \in [-100, 100]\,\text{mm}$ is the linear translation along the proximal axis. These equations form the basis for inverse kinematics, mapping workspace positions to joint commands. The resulting tip trajectories were tracked using two perpendicular cameras, with the reference position defined at $z = 0$ for consistency across trials. Both side and tip views were recorded for precise monitoring of tip motion (Fig. 7(b)–(c)). The accuracy assessment experiment results are shown in Fig. 8. Fig. 8(a) illustrates the complete reachable workspace of the ARA-URS, while Fig. 8(b) shows the 30 selected target points with a direct comparison of the desired versus tracked trajectories in both simulation and real-world execution. Fig. 8(c)–(e) provide orthogonal 2D projections of the target and actual positions, clearly visualizing positional deviations across different planes. Fig. 8(f) presents the tip tracking errors in the x, y, and z directions, quantitatively demonstrating the calibration accuracy of the system.

B. In-vitro Stone Targeting Experiment

Following the in-air kinematic assessment experiment, the real-world and DT models of the ARA-URS were further evaluated for task-oriented navigation through an in-vitro stone targeting experiment. In this setup, the tip of the ureteroscope was initially positioned in the renal pelvis approximately 2–3 cm from the kidney stone. From this starting point, the robotic system autonomously navigated

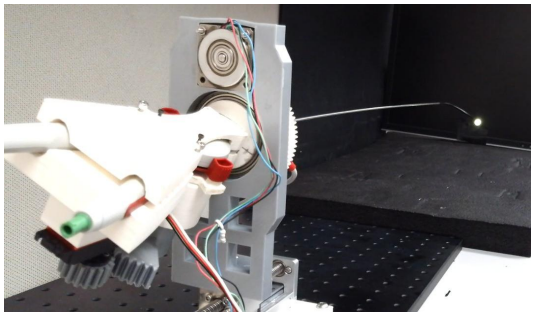

(a) In-air kinematic accuracy assessment expt. setup

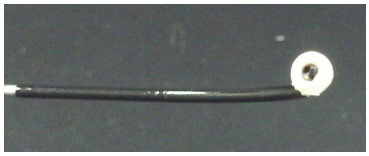

(b) Tip tracking from side view

(c) Top view

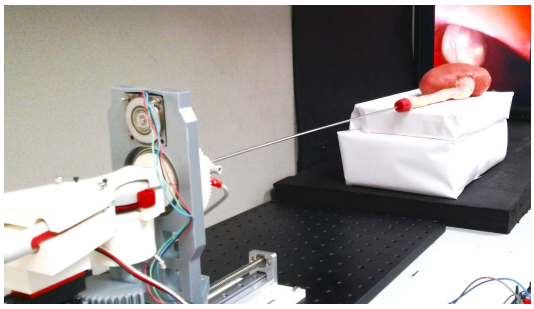

(d) In-vitro stone targeting experimental setup

Fig. 7: Experimental setup.

toward the stone until the ureteroscope tip reached the closest feasible position. Once the ureteroscope was placed in proximity, the stone was detected and masked using a vision pipeline, which enabled continuous tracking of the stone location during the experiment. The detected stone position was then used to guide the robot motion, allowing the system to converge toward the target and reach close proximity. This experimental working-space was selected to replicate the clinically relevant scenario where, once in close proximity, the ARA-URS must be able to move toward the stone and make subtle adjustments to ensure the stone is accessible for laser lithotripsy. To quantitatively assess targeting success, the stone coverage within the ureteroscopic camera frame was used as the primary metric. If the stone occupied 50% or more of the image frame, the trial was considered successful,

as this ensured sufficient visual dominance of the stone for safe and effective laser lithotripsy. This criterion was applied consistently across both DT and real-world experiments.

The experimental setup for in-vitro stone targeting is shown in Fig. 7(d), where the ureteroscope camera image of the stone positioned in front of it is displayed on the monitor. For the DT experiments, Fig. 9(i) illustrates the initial view of the stone, while Figs. 9(ii-xxxi) show the final targeted positions after the robotic navigation. Similarly, for the real-world setup, Fig. 10(i) shows the initial stone view, and Figs. 10(ii–xxxi) depict the corresponding post-targeting views. Representative examples of stone coverage are provided in Fig. 11, where Fig. 11(a) shows the area covered in the DT model and Fig. 11(b) presents the real-world results. In both cases, the average stone coverage exceeded the 50% threshold, confirming that the robotic system consistently guided the ureteroscope tip into clinically optimal positions for subsequent laser lithotripsy.

IV. Discussion

We investigated the kinematic accuracy and task-navigation capabilities of the ARA-URS system through two complementary experiments: In-air Kinematic accuracy assessment and In-Vitro Stone Targeting. The integration of real-world and DT models enabled a comprehensive evaluation of targeting precision and workspace reproducibility. Table I provides a quantitative performance summary of both experiments. In the In-air kinematic assessment experiment, 30 randomly distributed points were selected within the reachable workspace, and the corresponding joint variables were obtained via inverse kinematics (IK). The results demonstrated close agreement between DT and real-world trials, although notable deviations were observed in the latter. As shown in Table I, the root mean square errors (RMSE) along the (x, y, z) axes were [5.9856, 6.5434, 4.8734] mm, yielding a mean Euclidean error of 9.665 mm with a standard deviation of 2.998 mm.

TABLE I: Summary of simulated and real-world experimental results

In-air Kinematic Calibration	**Values [mm]**
Error RMSE (x, y, z)	[5.985, 6.543, 4.873]
Mean Eucli. error, and Std. dev.	[9.665, 2.998]
In-Vitro Stone Targeting	**Values [%]**
Average area coverage (DT)	88.77
Average area coverage (Real world)	58.94

Several factors contributed to the observed discrepancies:

1) The long and rigid ureteroscope shaft in the in-air configuration introduced mechanical vibrations at the distal tip, amplifying error.
2) Simultaneous actuation of the three joints (linear insertion, rotation, and tip bending) compounded vibration effects. In surgical conditions, however, the shaft typically remains in contact with the ureter wall or ureteral access sheath, which provides natural damping and is expected to reduce error.

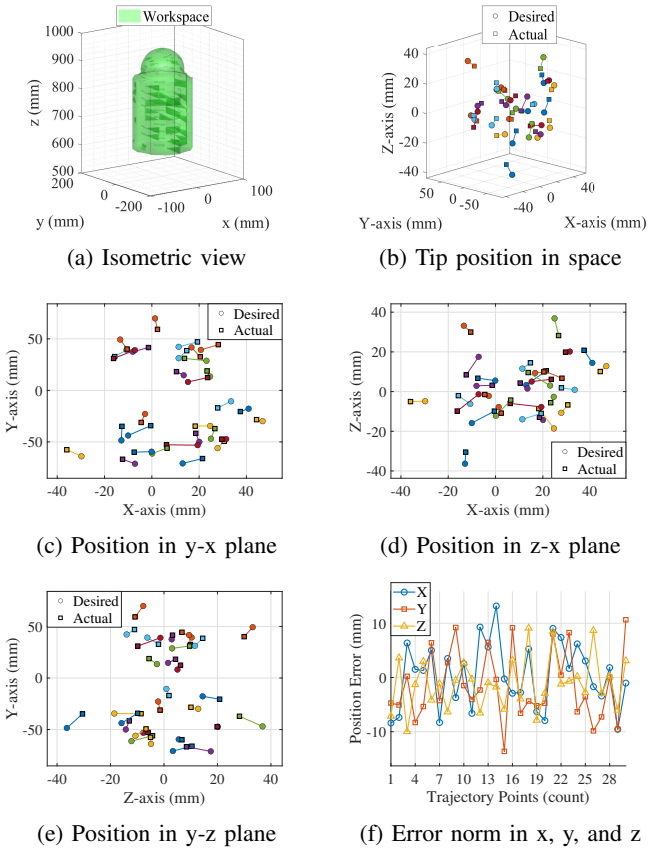

(a) Isometric view (b) Tip position in space

(c) Position in y-x plane (d) Position in z-x plane

(e) Position in y-z plane (f) Error norm in x, y, and z

Fig. 8: Total Workspace and Results of airborne tip positioning for a real world URS robot.

3) Optical tracking relied on a white PLA marker sphere mounted at the tip. This simplified detection but introduced additional tracking noise, particularly in the x and y directions.
4) Calibration was constrained to external camera-based monitoring.

Overall, these findings confirm that the DT environment accurately replicates the kinematics of the physical system, while highlighting sources of error specific to the In-air mechanical configurations.

The second experiment assessed the system's ability to autonomously navigate the ureteroscope tip toward a kidney stone for laser lithotripsy. The task began with the ureteroscope placed 2–3 cm from the stone, after which the DT and real-world systems executed IK-based motion to reach the closest point of approach. Targeting success was evaluated using stone coverage in the endoscopic image: if the stone occupied $\geq 50\%$ of the frame, the trial was considered successful for dusting and fragmentation readiness. It is important to point out that there exists no one perfect working distance in URS. However, to perform lithotripsy the laser must have adequate space to safely be advanced (so that the laser energy does not damage the ureteroscope) [27], but also if advanced too far, the fiber can become unstable and even break. Therefore, in our second experiment, we tested whether we could reach the kidney stone, at a minimum

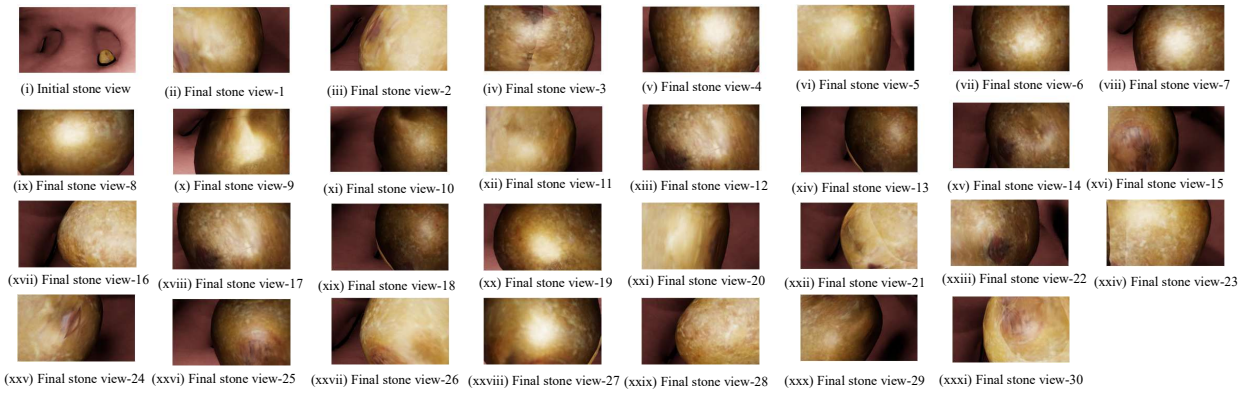

Fig. 9: Stone targeting in the DT. (i) Initial stone view, (ii-xxxi) post-targeting views after robotic vision-based navigation.

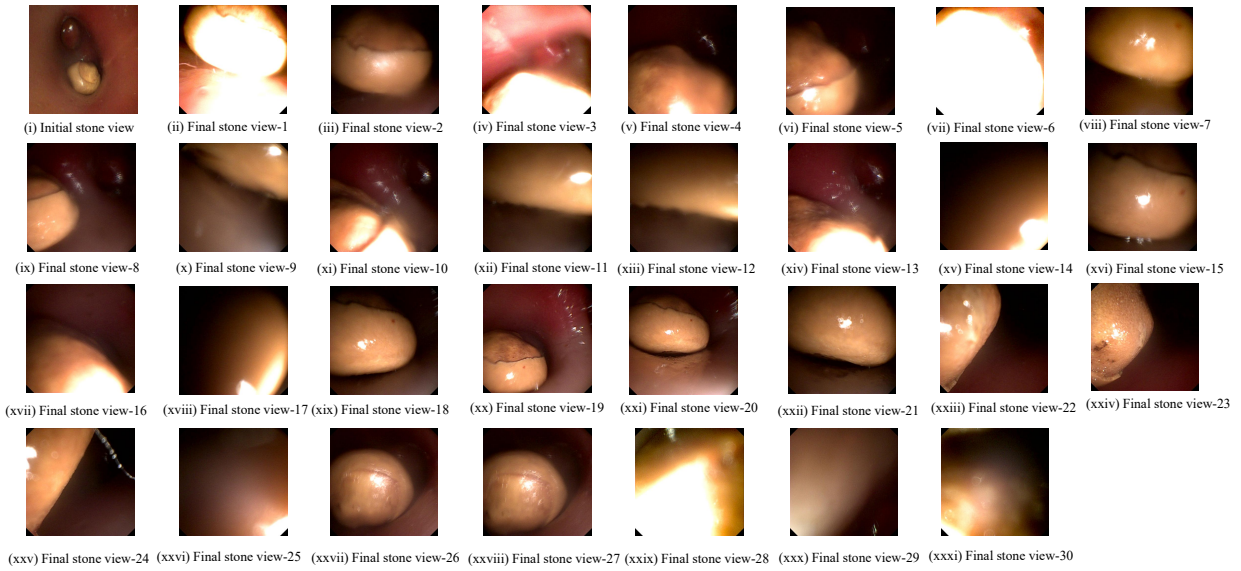

Fig. 10: Stone targeting in the real-world setup. (i) Initial stone view, (ii-xxxi) post-targeting views after robotic vision-based navigation.

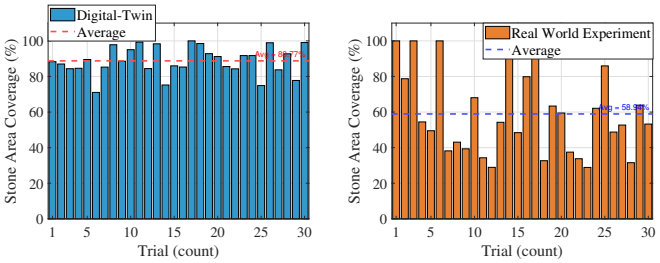

(a) In DT experiment (b) In real-world experiment

Fig. 11: Percentage of stone area covered in the ureteroscopic view. (a) DT setup, (b) real-world setup.

defined by reaching a safe working distance where the stone occupies half the screen, to facilitate future optimal laser lithotripsy. The quantitative results (Table I) show that the average stone coverage was 88.77% in simulation and 58.94% in real-world trials, both exceeding the success threshold. This confirms that the system mostly guided the ureteroscope tip into clinically acceptable positions for laser lithotripsy and never completely lost the stone. The small performance gap between simulation and real-world targeting is attributed to mechanical tolerances, camera distortions, and uncertainties in stone surface modeling.

The combined results underscore the feasibility of DT-assisted ARA-URS for surgical task execution. In both experiments, the DT consistently outperformed the real-world trials in terms of numerical accuracy, reflecting its ability to provide a near-idealized kinematic environment. The real-world deviations, while higher, remain within clinically acceptable bounds and provide insight into areas requiring refinement. Importantly, this work demonstrates that ARA-URS with a high-fidelity DT can serve as a powerful framework for automating kidney stone ureteroscopy, enabling accurate calibration, reliable stone targeting, and seamless mapping between simulation and physical execution.

V. Conclusion and Future Scope

This work presented a 3-DOF supervised autonomous robotic-assisted ureteroscopic system (ARA-URS) integrated

with a digital twin (DT) for kinematic accuracy assessment and task navigation. Two experimental studies – in-air kinematic accuracy assessment and in-vitro stone targeting – demonstrated that the DT is capable of reproducing the motion behavior of the physical system while enabling controlled evaluation of targeting performance. The results show that the DT environment can support development and validation of navigation strategies prior to deployment on the physical system. These findings highlight the feasibility of a DT-assisted RA-URS framework for improving experimental reproducibility, system evaluation, and training in minimally invasive kidney stone surgery.

Future work will focus on improving both the robotic system and the DT by incorporating physiological dynamics such as ureteral peristaltic motion, improving mechanical transmission to reduce vibration, and integrating advanced sensing technologies including electromagnetic tracking and fiber Bragg grating (FBG) sensors for more accurate tip localization. Additional studies will investigate dynamic stone motion, fluid-filled intra-renal conditions, and the reachability of the system across different regions of the renal collecting system. Expanding the diversity of kidney models in both physical and simulated environments will further improve the generalizability of the proposed framework.

Overall, this work provides a proof-of-concept for digital twin-assisted robotic ureteroscopy and establishes a foundation for the development of perception-driven, clinically relevant robotic assistance systems for kidney stone treatment.

ACKNOWLEDGMENT

The authors thank Xinrong Ye for help with 3D modeling of the robotic hardware, Nisan Korkmaz for kidney model rendering, and Kimberly Cortés Pérez and Luca Civetta for their assistance in developing the kidney stone models.

REFERENCES

[1] C. R. Haas, S. Li, M. A. Knoedler, K. L. Penniston, and S. Y. Nakada, "Ureteroscopy and Shock Wave Lithotripsy Trends from 2012 to 2019 Within the US Medicare Dataset: Sharp Growth in Ureteroscopy Utilization," *Journal of Endourology*, vol. 37, January 2023.

[2] T. H. C. d. Silva, C. C. Passerotti, J. PONTES, L. F. Maximiano, J. P. Otoch, and J. A. S. d. Cruz, "The learning curve for retrograde intrarenal surgery: A prospective analysis," *Revista do Colégio Brasileiro de Cirurgiões*, vol. 49, p. e20223264, 2022.

[3] K. R. G and J. S. W, "What is the stone-free rate following flexible ureteroscopy for kidney stones?," *Nature Reviews Urology*, vol. 12, May 2015.

[4] D. M. Lopategui, A. Bhatia, J. G. Porto, A. Rathinam, J. C. Daher, R. R. Chen, H. Haile, M. Ahumada, M. Meyreles, J. Katz, *et al.*, "Factors influencing computed tomography determined stone-free rates after ureteroscopy in real-world and its impact on retreatment rates at medium-term follow-up," *World journal of urology*, vol. 43, no. 1, p. 350, 2025.

[5] B. R. Matlaga, T. J. Mueller, B. Johnson, J. Page, J. S. Wolf Jr, G. M. Preminger, L. Jones, I. Sobol, K. Stern, D. Cuellar, *et al.*, "A prospective, randomized, noninferiority study to evaluate the safety and effectiveness of steerable ureteroscopic renal evacuation compared with standard ureteroscopy: 30-day results of the ASPIRE study," *Journal of endourology*, vol. 39, no. 1, pp. 10–18, 2025.

[6] D. A. Rebuck, A. Macejko, V. Bhalani, P. Ramos, and R. B. Nadler, "The natural history of renal stone fragments following ureteroscopy," *Urology*, vol. 77, no. 3, pp. 564–568, 2011.

[7] Chew *et al.*, "Natural history, complications and re-intervention rates of asymptomatic residual stone fragments after ureteroscopy: a report from the EDGE research consortium," *The Journal of urology*, vol. 195, no. 4 Part 1, pp. 982–986, 2016.

[8] T. Kanno, A. Matsuda, H. Sakamoto, Y. Higashi, and H. Yamada, "Safety and efficacy of ureteroscopy after obstructive pyelonephritis treatment," *International Journal of Urology*, vol. 20, September 2013.

[9] M. A. Elkoushy and S. Andonian, "Prevalence of orthopedic complaints among endourologists and their compliance with radiation safety measures," *Journal of endourology*, vol. 25, no. 10, pp. 1609–1613, 2011.

[10] G. Hellawell, S. Mutch, G. Thevendran, E. Wells, and R. Morgan, "Radiation exposure and the urologist: what are the risks?," *The Journal of urology*, vol. 174, no. 3, pp. 948–952, 2005.

[11] R. S. et al., "A new robot for flexible ureteroscopy: development and early clinical results (IDEAL stage 1-2b)," *European Urology*, vol. 66, December 2014.

[12] J. Park *et al.*, "The usefulness and ergonomics of a new robotic system for flexible ureteroscopy and laser lithotripsy for treating renal stones," *Investigative and Clinical Urology*, vol. 63, no. 6, p. 647, 2022.

[13] J. A. Cadeddu, "Re: A New Robot for Flexible Ureteroscopy: Development and Early Clinical Results (IDEAL Stage 1-2b)," *Journal of Urology*, 2015.

[14] J. Kim, H. Park, D.-S. Kwon, J. Y. Lee, and S. Y. Cho, "Robotic flexible ureteroscopy system, Zamenix R, demonstrates efficacy and safety in initial clinical evaluation for retrograde intrarenal surgery," *Scientific Reports*, vol. 15, no. 1, p. 17366, 2025.

[15] G.-Z. Yang, J. Cambias, K. Cleary, E. Daimler, J. Drake, P. E. Dupont, N. Hata, P. Kazanzides, S. Martel, R. V. Patel, *et al.*, "Medical robotics—Regulatory, ethical, and legal considerations for increasing levels of autonomy," *Science Robotics*, vol. 2, no. 4, p. eaam8638, 2017.

[16] N. Koenig and A. Howard, "Design and use paradigms for Gazebo, an open-source multi-robot simulator," in *IEEE/RSJ International Conference on Intelligent Robots and Systems (IROS)*, 2004.

[17] E. Todorov, T. Erez, and Y. Tassa, "MuJoCo: A physics engine for model-based control," in *2012 IEEE/RSJ International Conference on Intelligent Robots and Systems*, pp. 5026–5033, IEEE, 2012.

[18] T. D. Kainova, "Overview of the Accelerated Platform for Robotics and Artificial Intelligence NVIDIA Isaac," in *2023 Seminar on Information Computing and Processing (ICP)*, 2023.

[19] C. L. et al., "Simulation of a Total Knee Arthroplasty System Based on Extended Reality," in *2024 IEEE 12th International Conference on Serious Games and Applications for Health (SeGAH)*, vol. 26, 2024.

[20] A. Munawar, J. Y. Wu, G. S. Fischer, R. H. Taylor, and P. Kazanzides, "Open Simulation Environment for Learning and Practice of Robot-Assisted Surgical Suturing," *IEEE Robotics and Automation Letters*, vol. 7, 2022.

[21] "RIWOD-URS Richard Wolf richard-wolf.com." `https://www.richard-wolf.com/en-us/disciplines/urology/translate-to-english-usa-riwo-d-urs`. [Accessed 01-03-2025].

[22] D. Luo *et al.*, "Development and validation of a predictive model for failure of ureteral access sheath placement in patients with ureteral calculi," *BMC urology*, vol. 24, no. 1, p. 220, 2024.

[23] O. Traxer and A. Thomas, "Prospective evaluation and classification of ureteral wall injuries resulting from insertion of a ureteral access sheath during retrograde intrarenal surgery," *The Journal of urology*, vol. 189, no. 2, pp. 580–584, 2013.

[24] S. A. Setia, Z. A. Stoebner, C. Floyd, D. Lu, I. Oguz, and N. L. Kavoussi, "Computer vision enabled segmentation of kidney stones during ureteroscopy and laser lithotripsy," *Journal of Endourology*, vol. 37, no. 4, pp. 495–501, 2023.

[25] J. Leng, J. Liu, G. Cheng, H. Wang, S. Quarrier, J. Luo, and R. Jain, "Development of UroSAM: A Machine Learning Model to Automatically Identify Kidney Stone Composition from Endoscopic Video," *Journal of Endourology*, vol. 38, no. 8, pp. 748–754, 2024.

[26] D. Lu *et al.*, "ASSIST-U: A system for segmentation and image style transfer for ureteroscopy," *Healthcare Technology Letters*, vol. 11, no. 2-3, pp. 40–47, 2024.

[27] M. Talso, E. Emiliani, M. Haddad, L. Berthe, M. Baghdadi, E. Montanari, and O. Traxer, "Laser fiber and flexible ureterorenoscopy: the safety distance concept," *Journal of Endourology*, vol. 30, no. 12, pp. 1269–1274, 2016.